Antibacterial Activity of Graphite, Graphite Oxide, Graphene Oxide, and Reduced Graphene Oxide: Membrane and Oxidative Stress

Shaobin Liu,[†] Tingying Helen Zeng,[‡] Mario Hofmann,[§] Ehdi Burcombe,[§] Jun Wei,[⊥] Rongrong Jiang,[†] Jing Kong,[‡,§] and Yuan Chen[†,*]

[†]School of Chemical and Biomedical Engineering, Nanyang Technological University, Singapore 637459, [‡]Center for Excitonics, Research Laboratory of Electronics and [§]Department of Electrical Engineering and Computer Sciences, Massachusetts Institute of Technology, Cambridge, Massachusetts 02139, United States, and [⊥]Singapore Institute of Manufacturing Technology, Singapore 638075

ABSTRACT Health and environmental impacts of graphene-based materials need to be thoroughly evaluated before their potential applications. Graphene has strong cytotoxicity toward bacteria. To better understand its antimicrobial mechanism, we compared the antibacterial activity of four types of graphene-based materials (graphite (Gt), graphite oxide (GtO), graphene oxide (GO), and reduced graphene oxide (rGO)) toward a bacterial model—*Escherichia coli*. Under similar concentration and incubation conditions, GO dispersion shows the highest antibacterial activity, sequentially followed by rGO, Gt, and GtO. Scanning electron microscope (SEM) and dynamic light scattering analyses show that GO aggregates have the smallest average size among the four types of materials. SEM images display that the direct contacts with graphene nanosheets disrupt cell membrane. No superoxide anion ($O_2^{\bullet -}$) induced reactive oxygen species (ROS) production is detected. However, the four types of materials can oxidize glutathione, which serves as redox state mediator in bacteria. Conductive rGO and Gt have higher oxidation capacities than insulating GO and GtO. Results suggest that antimicrobial actions are contributed by both membrane and oxidation stress. We propose that a three-step antimicrobial mechanism, previously used for carbon nanotubes, is applicable to graphene-based materials. It includes initial cell deposition on graphene-based materials, membrane stress caused by direct contact with sharp nanosheets, and the ensuing superoxide anion-independent oxidation. We envision that physicochemical properties of graphene-based materials, such as density of functional groups, size, and conductivity, can be precisely tailored to either reducing their health and environmental risks or increasing their application potentials.

KEYWORDS: graphene · graphene oxide · reduced graphene oxide · bacterial cytotoxicity · membrane and oxidative stress

Graphene is a single atomic plane of graphite (Gt),[1,2] which was first obtained through micromechanical exfoliation of Gt.[3] Graphene oxide (GO) is a graphene sheet with carboxylic groups at its edges and phenol hydroxyl and epoxide groups on its basal plane.[4,5] GO can be chemically exfoliated from graphite oxide (GtO).[4] Thermal annealing or chemical treatment can eliminate functional groups on GO to produce reduced graphene oxide (rGO).[6] These graphene related materials exhibit unique electronic, thermal, and mechanical properties,[1,7] and hold great promises in potential applications, such as nanoelectronics, conductive thin films, supercapacitors, nanosensors and nanomedine.[2,8] To realize their potentials, health and environmental impacts of graphene related materials should be thoroughly evaluated. Compared to other synthetic carbon nanomaterials, such as fullerenes and carbon nanotubes (CNTs), few toxicity studies on graphene related materials are currently available.[9−12] Only recently, it was reported that GO and rGO exhibit strong antibacterial activity.[10,11] The antibacterial activity of GO and rGO has been attributed to membrane stress induced by sharp edges of graphene nanosheets, which may result in physical damages on cell membranes, leading to the loss of bacterial membrane integrity and the leakage of RNA.[11] On the other hand, it was proposed that graphene may induce oxidative stress on neural phaeochromocytoma-derived PC12 cells.[12]

The current few cytotoxicity studies on graphene-based materials suggest some similarity between graphene and other synthetic carbon nanomaterials. The antimicrobial activity of CNTs has been found to be the synergy of both "physical" and "chemical" effects.[13] When bacteria directly contact with CNTs, intensive physical interactions between CNTs and bacterial cells may cause physical damages on cell membranes, and result in the release of intracellular contents.[13,14] At the same time, some "small" CNTs could be internalized by bacterial cells, while other "larger" CNT aggregates may

* Address correspondence to chenyuan@ntu.edu.sg.

Received for review April 25, 2011 and accepted August 18, 2011.

Published online August 18, 2011
10.1021/nn202451x

stick on the surface of bacterial cells.[15−18] CNTs may chemically increase cellular oxidative stress, which could disrupt a specific microbial process.[13,14] If graphene-based materials share a similar antibacterial mechanism as that of CNTs, material characteristics which influence how graphene-based materials physically interact with bacterial cells, such as solubility, dispersion, and size, should strongly influence their antibacterial activities. Moreover, material properties, which control their abilities in producing cellular oxidative stress, should also have a strong impact on their antibacterial activities.

To better understand the health and environmental impacts of graphene related materials, the antibacterial activity of four types of graphene-based materials (Gt, GtO, GO, and rGO) toward a bacterial model—*Escherichia coli* (*E. coli*) was studied and compared. The time and concentration dependent antibacterial activities were found. Scanning electron microscopy (SEM) was applied to show different behaviors of GO and rGO dispersions toward bacterial cells. We first characterized graphene-based materials in aqueous dispersions by dynamic light scattering analysis (DLS), and then quantified their average sizes by SEM. The possibility of superoxide anion ($O_2^{\bullet-}$) induced reactive oxygen species (ROS) production was evaluated by the XTT method. *In vitro* glutathione (γ-L-glutamyl-L-cysteinyl-glycine, GSH) oxidation was used to examine the superoxide anion-independent oxidative stress. On the basis of these results, material characteristics related to their antibacterial activities were identified. We suggest that a three-step bacterial-cytotoxicity mechanism is applicable to graphene-based materials.

RESULTS AND DISCUSSION

Gt, GtO, GO, and rGO Dispersions. Gt, GtO, GO, and rGO were prepared as described in the Materials and Methods section. Photographs of Gt, GtO, GO, and rGO dispersions (at the concentration of 400 μg/mL) are shown in Figure 1a. They look differently because of their distinct structural and physicochemical properties. Black particles are visible in the Gt dispersion after sonication for 1 h. Most of Gt particles precipitated after the Gt dispersion stood still for 2 h. The GtO dispersion was obtained by the oxidation of Gt, and it is opaque yellow in color. Some small GtO particles can also be identified in the GtO dispersion. Significant portion of GtO particles precipitated after the GtO dispersion was idle for 2 h. However, if washed GtO powders were bath sonicated for 6 h, GO nanosheets were exfoliated from the GtO, resulting in the clear and homogeneous yellow-brown GO dispersion. The GO dispersion was stable after standing still for several days. This can be attributed to the large amount of hydrophilic functional groups, such as carboxyl, hydroxyl, and epoxy groups, on GO nanosheets.[19] Figure 1b

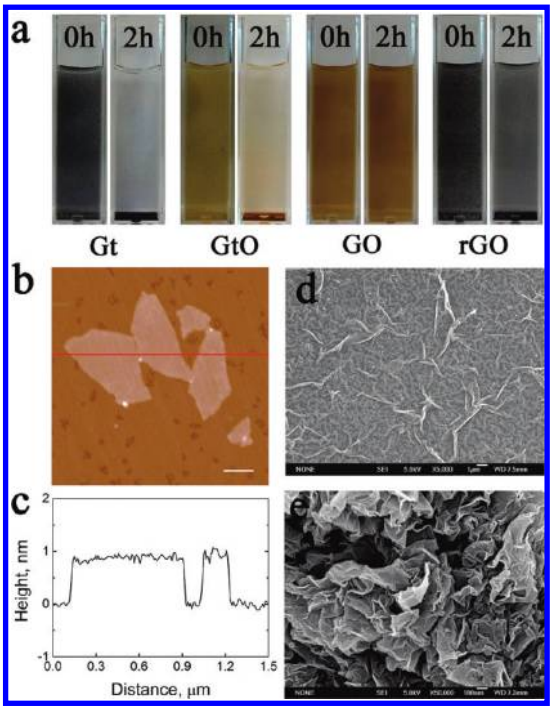

Figure 1. (a) Photographs of Gt, GtO, GO, and rGO dispersions (at the concentration of 400 μg/mL). Images marked "0h" show dispersions immediately after sonication, while images marked "2h" are from dispersions after standing still for 2 h. (b) AFM height image of GO nanosheets dried on a mica surface (the scale bar shows 200 nm) and (c) the corresponding height profile of the AFM image. (d, e) SEM images of GO (d) and rGO (e) nanosheets dried on silicon wafers.

shows an atomic force microscopy (AFM) image of GO nanosheets dried on a mica surface. The thickness of them is around 1 nm (see the AFM profile in Figure 1c); indicating single-layer GO sheets were produced. Figure 1d is an SEM image of dried GO sheets on a silicon wafer. GO sheets are smooth with small wrinkles at the edges. GO sheets were also characterized by Raman spectroscopy and X-ray photoelectron spectroscopy (XPS). Figure S1 in the Supporting Information shows a representative Raman spectrum of graphene oxide (GO) nanosheets used in this study. There are broad G and D band peaks. The intensity ratio of the D and G band (I_D/I_G) is 1.36 for our GO samples. In addition, there are three Raman bands with weaker but recognized features and intensity, called G′, D+G, and 2D′ bands, locating at 2700−3200 cm^{-1}. These Raman features suggest that graphene sheets changed to be more amorphous and defective upon exfoliation of Gt flakes. XPS analysis of carbon components in GO samples, shown in Supporting Information, Figure S2 and S3, indicates the ratio of carbon atoms in the perfect graphene sheet to those in lattice defects is 1:1. This high defect density agrees with the result obtained by Raman spectroscopy. The rGO dispersion was obtained by chemically reducing the GO dispersion using hydrazine.[19] After reduction, the surface of rGO nanosheets became hydrophobic, and some black

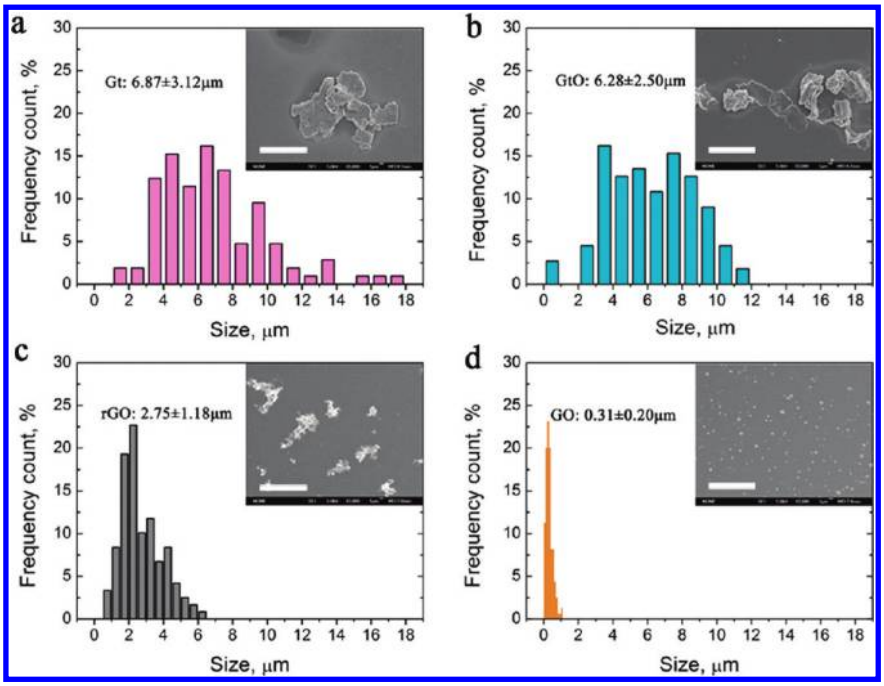

Figure 2. Size distributions of Gt (a), GtO (b), rGO (c), and GO (d). At least 200 particles were measured for each sample to obtain the size distribution. Inserts show their representative SEM images by drying Gt, GtO, rGO, and GO dispersions (at the concentration of 400 μg/mL) on clean silicon wafers. Scale bars are at 10 μm.

particles started precipitating.[19] The strong van der Waals forces among rGO nanosheets would facilitate the aggregation of rGO particles. Thus, plenty of rGO particles precipitate after the rGO dispersion stood still for 2 h. Figure 1e shows an SEM image of dried rGO sheets, and the rGO sheets are much rougher compared with GO sheets.

Aggregation of engineered nanomaterials exists commonly in aquatic systems,[20] including carbon nanomaterials, such as CNTs[21,22] and fullerene.[23,24] Different aggregation conditions could significantly influence the interaction between nanoparticles and bacteria.[18,25−28] Aqueous dispersions of Gt, GtO, GO, and rGO were first characterized by DLS. The standard spherical particle models were used in DLS. As shown in Supporting Information, Figure S4, the nominal effective diameters of particles in Gt, GtO, GO, and rGO dispersions are 5.25, 4.42, 0.56, and 2.93 μm, respectively. Because most of graphene-based materials are not spherical particles, the model derived diameters are not their real sizes. DLS results only show size differences among the four materials. The dispersions were further dropped on silicon wafers, and dozens of SEM images were taken randomly for each sample. The size distribution of Gt, GtO, GO, and rGO was determined by analyzing their SEM images using the Image J software from National Institutes of Health. As shown in Figure 2, the nominal size of Gt, GtO, GO, and rGO particles are 6.87 $\pm$ 3.12, 6.28 $\pm$ 2.50, 0.31 $\pm$ 0.20, and 2.75 $\pm$ 1.18 μm, respectively. Among them, GO nanosheets have the smallest size. Although GtO particles have similar chemical functionality as GO nanosheets, their average size is nearly 20 times larger than that of GO nanosheets. The rGO particles were formed by reducing GO nanosheets, and their size is about nine times larger than that of GO nanosheets because of the aggregation of rGO fragments. It also should be noted that GO consists of two-dimensional carbon sheets. Although the size of GO sheets measured by SEM are nearly 300 nm, their thickness is less than 1 nm, as shown in Figure 1c. On the other hand, Gt, GtO, and rGO would aggregate into three-dimensional micrometer scale particles.

Antibacterial Activity of Gt, GtO, GO, and rGO Dispersions. *E. coli* was used as a model bacterium to evaluate antibacterial activities of the four types of graphene-based materials. *E. coli* cells (10^6 to 10^7 CFU/mL) were incubated with the same concentration (40 μg/mL) of Gt, GtO, GO, and rGO dispersions in isotonic saline solution for 2 h, respectively. The death rate of bacterial cells was determined by the colony counting method described in the Materials and Methods section. The isotonic saline solution without graphene-based materials was used as a control. Control data in Supporting Information, Figure S5a show that the incubation conditions would not affect the cell viability assay. As shown in Figure 3a, the Gt dispersion exhibits a moderate cytotoxicity with the cell inactivation percentage at 26.1 $\pm$ 4.8%. The GtO dispersion shows a slight weaker antibacterial activity compared with Gt, having the cell inactivation percentage at 15.0 $\pm$ 3.7%. GO have a much stronger bacterial activity compared with GtO. The loss of *E. coli* viability increases to 69.3 $\pm$ 6.1%, which is more than 4-fold compared with that of

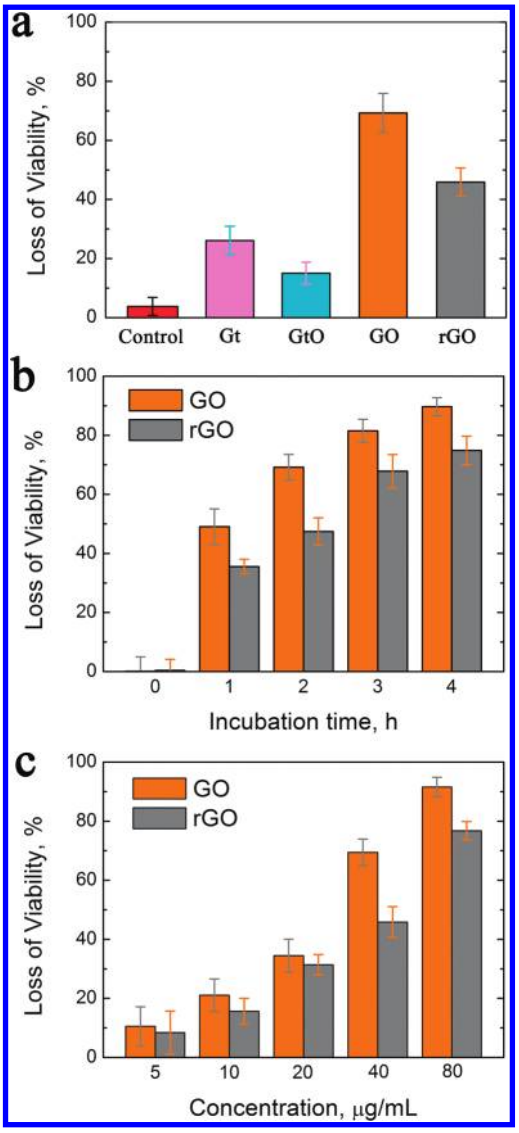

Figure 3. (a) Cell viability measurement after incubation with Gt, GtO, GO, and rGO dispersions. A 5 mL portion of graphene-based materials (80 μg/mL) was incubated with *E. coli* (10^6 to 10^7 colony forming units per milliliter (CFU/mL), 5 mL) for 2 h at 250 rpm shaking speed and 37 °C. Loss of cell viability rates was obtained by colony counting method. Error bars represent the standard deviation. Isotonic saline solution without graphene-based materials was used as control. (b) Time-dependent antibacterial activities of GO and rGO; 5 mL of GO or rGO (80 μg/mL) was incubated with *E. coli* (10^6 to 10^7 CFU/mL, 5 mL) for 4 h. The loss of visibility was measured at 0, 1, 2, 3, and 4 h, respectively. Isotonic saline solution without graphene-based materials was used as control, and the control data were provided in Figure S5a. (c) Concentration−dependent antibacterial activities of GO and rGO; 5 mL of GO or rGO (at 10, 20, 40, 80, and 160 μg/mL) was incubated with *E. coli* (10^6 to 10^7 CFU/mL, 5 mL) for 2 h.

GtO. rGO has a lower antibacterial activity compared with GO with a bacterial inactivation percentage of 45.9 ± 4.8%. Significant differences were found in their antibacterial activities among the four materials. In particular, GO and rGO have much higher bacterial inactivation percentages compared with those of Gt and GtO. It also should be noted that the shaking speed of 250 rpm was used in all antibacterial assays. Although some Gt, GtO, and rGO particles precipitate when the dispersions stand still for 2 h (shown in Figure 1), under the shaking condition, the particles are well suspended in the saline solution interacting with cells in all assays.

Time-Dependent and Concentration-Dependent Antibacterial Activity. Next, we examined the time−dependent antibacterial behavior of two materials (GO and rGO), which showed higher activities in our early tests. GO or rGO dispersions (40 μg/mL) were incubated with *E. coli* for 4 h. The loss of *E. coli* viability was counted at hourly intervals. Figure 3b indicates the loss of *E. coli* viability steadily increases with extending incubation time. For GO dispersion, the loss of *E. coli* viability increases from 49.1 ± 6.0% after 1 h incubation to 69.3 ± 6.1% after 2 h, and further increases to 81.5 ± 3.9% after 3 h and 89.7 ± 3.1% after 4 h. rGO dispersion displays a similar trend. The loss of *E. coli* viability is 35.6 ± 2.5% after 1 h, and increases to 47.4 ± 4.6, 67.8 ± 5.6, and 74.9 ± 4.8% after 2, 3, and 4 h, respectively. For both materials, a large fraction of cell death occurs in the first hour of incubation. Comparing GO and rGO dispersions, GO dispersions have much higher antibacterial activities than rGO dispersions at all tested incubation intervals.

Furthermore, the concentration dependence of antibacterial activities on graphene-based materials was studied. GO or rGO dispersions at different concentrations (5, 10, 20, 40, and 80 μg/mL) were incubated with *E. coli* cells (*ca.* 10^6−10^7 CFU/mL) for 2 h at 37 °C under the 250 rpm shaking speed. As shown in Figure 3c, the loss of *E. coli* viability progressively goes up with the increases of GO or rGO concentration. The loss of *E. coli* viability jumps from 10.5 ± 6.6% at the GO concentration of 5 μg/mL to 91.6 ± 3.2% at 80 μg/mL. The majority of *E. coli* was killed after incubation with GO at the concentration of 80 μg/mL. In a similar manner, rGO dispersion at the concentration of 5 μg/mL kills only 8.4 ± 7.3% of *E. coli*, while 80 μg/mL rGO dispersion kills 76.8 ± 3.1% of *E. coli*. These results suggest that antibacterial activities of graphene-based materials are also concentration dependent.

Destruction of Bacterial Membrane. To find out how graphene-based materials kill bacteria, SEM was used to illustrate interactions between graphene-based materials and *E. coli* cells. Figure 4 shows most of *E. coli* cells become flattened, and lose their cellular integrity after exposure to GO or rGO dispersions. The destruction of cells in SEM images is consistent with previous images obtained by transmission electron microscope.[10] It highlights that irreversible damages can be induced on bacterial cells after direct contact with graphene-based materials. This is similar to CNTs, which induce membrane stress on bacterial cells, resulting in destruction of cell structures. Besides, we observed that thin layers of nanosheets form GO dispersion, while rGO dispersion mainly contains large aggregated particles. A comparison of cells interacting with GO and

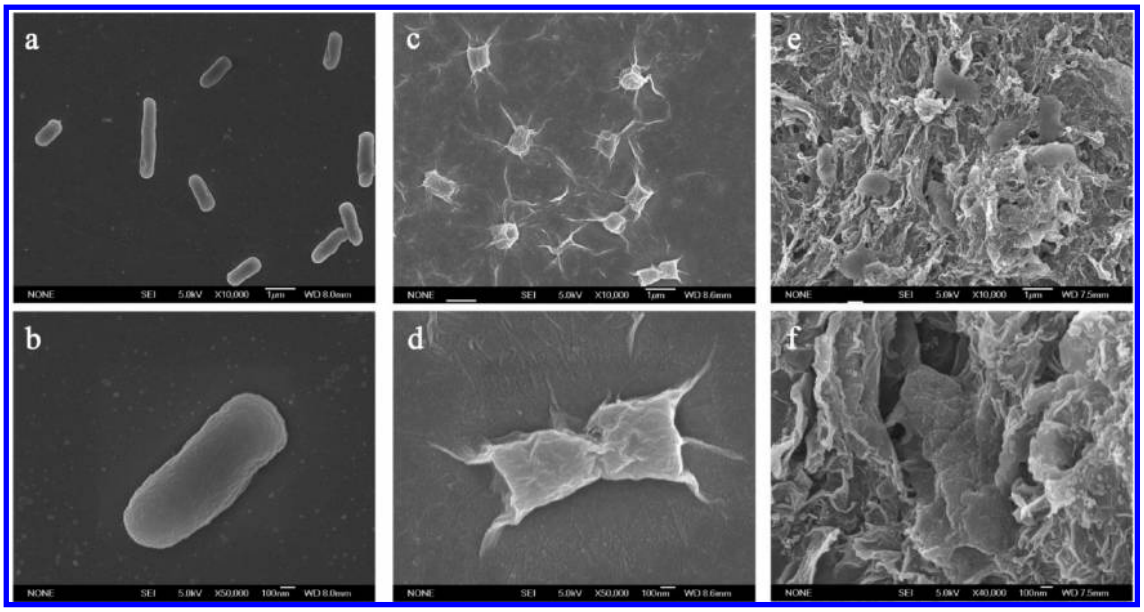

Figure 4. SEM images of (a, b) *E. coli* after incubation with saline solution for 2 h without graphene-based materials, (c, d) *E. coli* cells after incubation with GO dispersion (40 μg/mL) for 2 h, (e, f) *E. coli* cells after incubation with rGO dispersion (40 μg/mL) for 2 h.

rGO shows that *E. coli* mingle with GO and rGO in different manners. Figure 4 panels c and d show most of *E. coli* cells were individually wrapped by thin layers of GO nanosheets. In contrast, *E. coli* cells were usually embedded in large rGO aggregates (Figure 4e,f). The different behavior of GO and rGO observed in SEM images suggests the aggregation/dispersion of graphene-based materials may play an important role in their antibacterial activities.

Oxidative Stress Mediated by Gt, GtO, GO, and rGO. Other than membrane stress mediated by direct physical contacts, a previous study on graphene cytotoxicity has cited oxidative stress as its toxicity mechanism toward neural cells.[12] Oxidative stress is also often suggested as a key antibacterial mechanism of other carbon nanomaterials, such as fullerene[29,30] and CNTs.[13,14] Because of the similarity in their structural and physiochemical properties among these carbon nanomaterials, it is necessary to find out what cellular oxidative stress may be produced by Gt, GtO, GO, and rGO.

In general, oxidative stress mediated by graphene-based materials may come from several paths, one is reactive oxygen species (ROS) mediated oxidative stress, in which oxidative stress is induced by ROS generated by Gt, GtO, GO, and rGO. This is the mechanism proposed in the previous graphene toxicity study.[12] The other possible path is ROS-independent oxidative stress, in which graphene-based materials may disrupt a specific microbial process by disturbing or oxidizing a vital cellular structure or component without ROS production. This path has been observed in fullerene (C_{60}).[30] To better clarify different oxidative stress paths, we first measured the possibility of superoxide anion ($O_2^{\bullet-}$) production using the XTT method as described in the Materials and Methods section. Shown in Supporting Information, Figure S6,[31] no noticeable absorption is detected during the entire 5 h incubation period, which indicates that no $O_2^{\bullet-}$ is produced. TiO_2 under UV radiation as a positive control validated our XTT tests. On the basis of the XTT results, we conclude that graphene-based materials mediate little superoxide anion production. Previous studies indicated that some other ROS (such as singlet oxygen and hydroxyl radical) can derive from superoxide anions.[32,33] Our current results based on superoxide anion production suggest that although trace amount of ROS may be produced, it plays a minor role in the antibacterial activity of graphene-based materials. Nevertheless, the production and impact of different possible ROS should be carefully examined in future studies.

Next, we used *in vitro* GSH oxidation to examine the possibility of ROS-independent oxidative stress mediated by Gt, GtO, GO, and rGO dispersions. GSH is a tripeptide with thiol groups. It is an antioxidant in bacteria at a concentration ranging between 0.1 and 10 mM.[34] GSH can prevent damages to cellular components caused by oxidative stress.[35] Thiol groups (−SH) in GSH can be oxidized to disulfide bond (−S−S−), which converts GSH to glutathione disulfide. GSH has been used as an oxidative stress indicator in cells.[13,29,36] The Ellman's assay is able to quantify the concentration of thiol groups in GSH.[37] As described in the Materials and Methods section, we employed the Ellman's assay to evaluate the oxidation of GSH when it was incubated with Gt, GtO, GO, or rGO dispersions (40 μg/mL). Bicarbonate buffer (50 mM at pH 8.6) without graphene-based materials were used as control in GSH oxidation experiments. The control data in Supporting

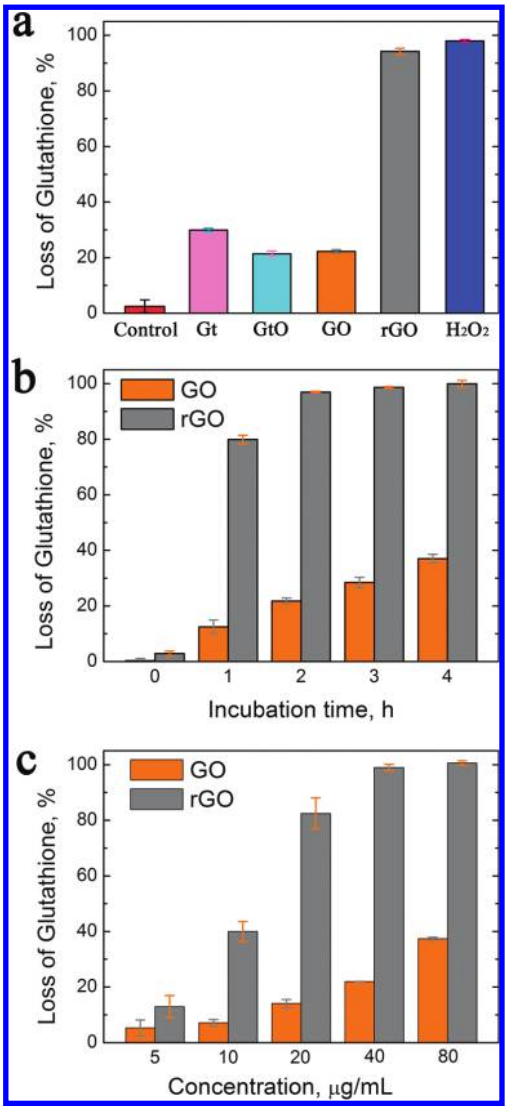

Figure 5. Oxidation of glutathione by graphene-based materials: (a) loss of GSH (0.4 mM) after *in vitro* incubation with 40 μg/mL of Gt, GtO, GO, and rGO dispersions for 2 h. H_2O_2 (1 mM) is a positive control. The bicarbonate buffer (50 mM at pH 8.6) without graphene-based materials was used as a negative control. (b) Time dependent GSH (0.4 mM) oxidation by GO and rGO dispersions (40 μg/mL) after incubation from 0 to 4 h. The bicarbonate buffer (50 mM at pH 8.6) without graphene-based materials was used as a negative control, and the control data were provided in Supporting Information, Figure S5b. (c) Concentration dependent GSH (0.4 mM) oxidation by GO and rGO (at 5, 10, 20, 40, and 80 μg/mL) after incubation for 2 h.

Information Figure S5b suggest that our incubation conditions would not cause GSH oxidation. As shown in Figure 5a, a noteworthy fraction of GSH is oxidized after its exposure to Gt (29.9 $\pm$ 0.7%), GtO (21.4 $\pm$ 1.1%), GO (22.2 $\pm$ 0.7%), and rGO (94.2 $\pm$ 1.1%). Among the four types of graphene-based materials, rGO has the highest oxidation capacity toward GSH, followed by Gt. GtO and GO have lower GSH oxidation capacities. A previous study has shown that the GSH oxidation by single walled carbon nanotubes (SWCNTs) depends on the metallicity of SWCNTs. The extent of GSH oxidation was observed to increase with increasing fraction of metallic nanotubes in SWCNT samples.[13] Different oxidation capacities toward GSH among Gt, GtO, GO, and rGO can be also attributed to their different electronic properties. Gt is an electrical conductor, a semimetal. When GtO and GO are oxidized from Gt by introducing functional groups, sp^2 hybridized electron structure of the stacked graphene sheets was broken.[38] In contrast, GtO and GO are electrically insulating materials. If GO is reduced, the π electron network of graphene can be partially restored.[39] Graphene is a zero-gap semiconductor with excellent electrical conductivity.[2] Conductivity of rGO is much higher than GtO and GO. Materials with higher conductivity, such as rGO and Gt, do show higher oxidation capacities to GSH, compared with materials with lower conductivity, such as GtO and GO. Our observation suggests that rGO may share the similar mechanism as metallic SWCNTs. They could act as a conductive bridge over the insulating lipid bilayer to release cellular energy ($GSH \rightarrow GSSG + 2e^- + 2H^+$) into the external environment ($O_2 + 2e^- + 2H^+ \rightarrow H_2O_2$).[13]

Because cell viability tests have shown that the antibacterial activities of graphene-based materials are time and concentration dependent (see Figure 3b,c), we speculate the oxidation of GSH by these materials should be time and concentration dependent as well. GSH oxidation by GO and rGO was compared over different periods of time and under several concentrations. When 0.4 mM GSH was incubated with 40 μg/mL GO or rGO, the oxidation of GSH gradually advance with extending reaction time. Figure 4b shows the fraction of GSH oxidized by rGO increases from 79.9 $\pm$ 1.6 to 99.9 $\pm$ 1.2% when the reaction time increase from 1 to 4 h. Likewise, over the same period of time, the oxidation of GSH by GO goes up from 12.5 $\pm$ 2.4 to 37.0 $\pm$ 1.5%. A large fraction of GSH is oxidized in the first 1 h of incubation. GSH (0.4 mM) was also incubated with different concentrations of GO or rGO (5–80 μg/mL) for 2 h. Figure 5c shows oxidizing GSH by rGO and GO is also concentration dependent. rGO oxidized 13.0 $\pm$ 4.0% of GSH at 5 μg/mL and all GSH (99.0 $\pm$ 1.1%) at 80 μg/mL. GO oxidized 5.3 $\pm$ 2.9 and 22.0 $\pm$ 0.1% of GSH at 5 and 80 μg/mL, respectively. Comparably, rGO has significantly higher oxidation reactivity than GO at the same reaction time and concentration. On the whole, more GSH are oxidized with the increase of reaction time and rGO/GO concentration, which is consistent with the time and concentration dependent incremental trend observed in the antibacterial activities of rGO and GO. The oxidation of GSH indirectly confirms that graphene-based materials are capable of mediating ROS-independent oxidative stress toward bacterial cells.

Antibacterial Mechanism of Gt, GtO, GO, and rGO. The correlation among antibacterial activities, GSH oxidation and aggregate size is summarized in Table 1, which can be examined from three aspects. First,

TABLE 1. The Correlation among Antibacterial Activities, Oxidative Stress, and Particle Size

	loss of cells[a] (%)	loss of GSH[b] (%)	particle size[c] (μm)
GtO	15.0 ± 3.7	21.4 ± 1.1	6.28 ± 2.50
Gt	26.1 ± 4.8	29.9 ± 0.7	6.87 ± 3.12
rGO	45.9 ± 4.8	94.2 ± 1.1	2.75 ± 1.18
GO	69.3 ± 6.6	22.2 ± 0.7	0.31 ± 0.20

[a] Data extracted from Figure 3a. [b] Data extracted from Figure 5a. [c] Data extracted from Figure 2.

comparing GtO and GO, they have similar capacities in oxidizing GSH (GtO at 21.4 ± 1.1% *vs* GO at 22.2 ± 0.7%); however, GO dispersion can kill much higher fractions of *E. coli* (69.3 ± 6.6%) than GtO dispersion (15.0 ± 3.7%). GtO and GO contain almost the same chemical functional groups. Their difference is that GO is individual nanosheets with average size of 0.31 ± 0.20 μm, while GtO is aggregated stacks of GO nanosheets with average particle size of 6.28 ± 2.50 μm. Their distinct antibacterial activities suggest the aggregation of graphene nanosheets is important in the antibacterial mechanism. Materials having smaller size (*e.g.*, GO), have higher cytotoxicity than those with larger size (*e.g.*, GtO). This size dependent toxicity is similar to what has been observed on CNTs.[14] Smaller diameter SWCNTs have higher antibacterial activity than larger diameter multiwall carbon nanotubes (MWCNTs).[14] Second, comparing Gt and GtO, Gt particles (6.87 ± 3.12 μm) are slightly larger than GtO particles (6.28 ± 2.50 μm). However, we found the antibacterial activity of Gt (26.1 ± 4.8%) is much higher than that of GtO (15.0 ± 3.7%). This is obviously correlated with their different GSH oxidation capacities. Metallic Gt can oxidize more GSH than insulating GtO, suggesting that the metallicity of graphene materials also plays a role in their antibacterial activities. Third, if we compare GO with rGO, although rGO shows much stronger oxidation capacity toward GSH, smaller size GO has much higher antibacterial activity than rGO. Overall, results in Table 1 suggest the antibacterial activities of graphene-based materials are attributed to their dispersibility, size, and oxidization capacity. Their antibacterial mechanism is likely to be the synergy of membrane stress and oxidative stress.

Vecitis *et al*. have previously proposed a three-step cytotoxicity mechanism for SWCNTs.[13] The first step is bacterial adhesion or deposition onto SWCNTs resulting in direct bacterium−SWCNT contact. The second step is that SWCNT would make intimate, membrane disruptive interaction with bacteria, inducing membrane stress. The third step involves disrupting a specific microbial process by disturbing or oxidizing a vital cellular structure or component. We reason that this three-step toxicity mechanism is also applicable to graphene-based materials. *E. coli* cells may first deposit on Gt, GtO, GO, or rGO during incubation. The dispersibility and size of materials should strongly influence the chance of cell deposition. In general, the dispersibility of graphene-based materials depends on functional groups on graphene sheets. When carboxyl, hydroxyl, and epoxy groups are introduced on graphene sheets, they form much more stable dispersions compared with hydrophobic pristine carbon planes. GO can form stable dispersions with small nanosheets, thus offers more opportunities to interact with cells for cell deposition. Comparably, Gt and rGO dispersions are unstable, and contain large particles; thus, they have fewer chances to mingle with cells. Similar phenomena have been previously observed on other carbon nanomaterials. For instance, surfactant dispersed individual SWCNTs shows higher toxicity to various bacterial cells than nanotube aggregates.[27] Functioned and debundled CNTs display stronger toxicity compared with as-synthesized CNT aggregates.[26] Small nC_{60} aggregates also show higher bacterial toxicity than large aggregates.[25]

After cell deposition on graphene nanosheets, the sharp edge of graphene nanosheets may cause significant membrane stress.[11] Nanosheets serve as "cutters" to disrupt and damage cell membranes, leading to the release of intracellular contents, and eventually cell death. SEM images in Figure 4 show the disruption role of graphene nanosheets. A notable difference among different graphene materials is that small GO nanosheets can wrap bacterial cells, while large rGO aggregates would trap cells. A molecular simulation has recently confirmed that small graphene sheets ($\sim$5.9 × 6.2 nm^2) can be trapped in biological membranes consisting of phospholipid molecules.[40] It is likely that some graphene nanosheets may be internalized by bacterial cells, as previously observed on A549 cells.[10] Although we found that few superoxide anions were generated by graphene-based materials, GSH oxidation (Figure 5) indicates that the oxidation capacity of graphene-based materials may play a significant role when nanosheets are in direct contact with cellular components. A comparable case is that metallic SWCNTs can act as a conducive bridge over the insulating lipid bilayer, mediating electron transfer from bacterial intracellular components to the external environments.[13] By analogy, graphene-based materials could also oxidize bacterial lipids, proteins, and DNA. The strong oxidation of GSH by rGO observed in our study supports that conductive graphene nanosheets are capable of oxidizing thiols or other cellular components.

Kinetic Analysis of Cell Inactivation and GSH Oxidation. To further evaluate the aforementioned antibacterial mechanism, the cell inactivation and GSH oxidation were compared through quantitative kinetic data extracted from Figures 3 and 5. The time dependent rate changes are presented in Figure 6a. During the first 2 h of incubation, even though rGO has much higher GSH

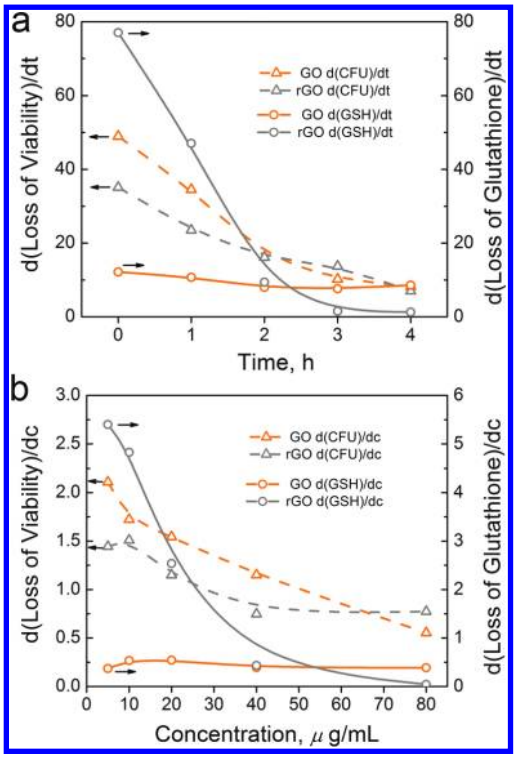

Figure 6. (a) The time dependent *E. coli* cell inactivation and GSH oxidation rates after incubated with GO and rGO dispersions, which are extracted from Figures 3b and 5b with the unit of d(%)/d(h). (b) The dependence of *E. coli* cell inactivation and GSH oxidation on GO and rGO concentrations, which are extracted from Figures 3c and 5c with the unit of d(%)/d(μg/mL).

oxidation rate than GO, its cell inactivation rate is still lower than that of GO. This corroborates the importance of the initial deposition of graphene-based materials on cell surfaces. Without direct interactions with bacterial cells, the stronger oxidation capacity of rGO does not result in the stronger antibacterial activity. Furthermore, the GSH oxidation rate of GO shows minor changes over the 4 h incubation, while the cell inactivation rate decreases continuously. This suggests that the membrane stress inducted by graphene-based materials may play more important roles during the first 2 h, while oxidative stress could become more prominent when bacterial cells have been covered by graphene-based materials in the last 2 h. Figure 6b illustrates the dependence of cell inactivation and GSH oxidation on GO and rGO concentrations. All incubations were fixed at 2 h. The GSH oxidation by rGO is more sensitive to the rGO concentration compared with the GSH oxidation by GO. However, the dependence of cell inactivation on concentration is similar between GO and rGO. It provides a circumstantial evidence that the antibacterial activity of graphene materials is contributed by both membrane and oxidation stress. Overall, the kinetic analysis results support the proposed antibacterial mechanism.

CONCLUSION

The antibacterial activity of Gt, GtO, GO, and rGO aqueous dispersions toward *E. coli* was compared. Colony counting method results show that GO has the highest antibacterial activities, followed by rGO, Gt, and GtO under the same dispersion concentration. Their antibacterial activities are time and concentration dependent. Most of bacterial inactivation happens in the first hour of incubation, and cell death rate increases continuously with the increase of material concentration. The bacterial cytotoxicity may be attributed to both membrane and oxidative stress. A three-step antibacterial mechanism is applicable to graphene-based materials. In general, graphene materials, which contain a higher density of functional groups, and are smaller in size, have more chances to interact with bacterial cells, resulting in cell deposition. By direct contact, graphene nanosheets can induce membrane stress by disrupting and damaging cell membranes, leading to cell death. The XTT tests show that no superoxide anions are produced by Gt, GtO, GO, and rGO. On the other hand, they display strong time- and concentration-dependent oxidization capacity toward GSH. The oxidation of GSH suggests that these graphene-based materials are capable of inducing superoxide anion-independent oxidative stress on bacterial cells. If they are in direct contact with cells, conductive rGO and Gt would mediate more intense oxidative stress compared with insulating GO and GtO. With the knowledge obtained in this study, we envision that physicochemical properties of graphene-based materials, such as the density of functional groups, size, and conductivity, can be better tailored to either reducing their risks or increasing their application potentials.

MATERIALS AND METHODS

Preparation and Characterization of Gt, GtO, GO and rGO Dispersions. Gt dispersion was obtained by sonicating graphite powders (Aldrich, synthetic, <20 μm) in isotonic saline solution (0.9 w/v % NaCl) using a bath sonicator (Elamsonic, S60H) at 37 kHz under 550 W for 1 h. GtO was prepared by the modified Hummers method as described in the Supporting Information.[41,42] As-produced GtO was first thoroughly washed using deionized water to remove chemical residues. GtO dispersion was then prepared by dispersing washed GtO in saline solution by shaking with vortex. GO was produced by bath sonicating washed GtO powder in water at 550 W for 6 h. rGO was obtained by hydrazine reduction as described in the Supporting Information,[19] and dispersed in saline solution by bath sonication at 550 W for 1 h. Gt, GtO, GO, and rGO dispersions with different concentrations were prepared by dispersing specific amount of solid powders in saline solution. The four types of graphene-based samples were characterized by various techniques. Dispersion (3 μL) was dropped on freshly cut mica

followed by air drying for AFM analysis. AFM analysis was performed on an MFP3D microscope (Asylum Research, Santa Barbara, CA) with a cantilever (Arrow NC, Nanoworld) in AC mode. Raman spectra of GO samples were obtained using a laser excitation of 532 nm at a power of <1 mW. The carbon-related chemical component species of GO were characterized by high resolution XPS using a Kratos Axis Ultra DLD (delay line detector) spectrometer equipped with a monochromatic Al Ka X-ray source (1486.69 eV). Various dispersions at the concentration of 400 μg/mL were also dried on clean silicon wafers and then viewed on a JEOL field emission SEM (JSM-6700F), working at 5 kV. The distribution of Gt, GtO, rGO, and GO was determined by analyzing SEM images using the Image J software (National Institutes of Health). At least 200 particles were measured for each sample. The particle size of dispersions was also measured by DLS on a ZetaPALS particle size analyzer (Brookhaven) at the scattering angle $\theta = 90°$.

Cell Preparation. *E. coli* K12 were grown in LB (Luria−Bertani) medium at 37 °C, and harvested in the midexponential growth phase. Cultures were centrifuged at 6000 rpm for 10 min to pellet cells, and cells were washed three times with isotonic saline solution to remove residual macromolecules and other growth medium constituents. The pellets were then resuspended in isotonic saline solution. Bacterial cell suspensions were diluted to obtain cell samples containing 10^6 to 10^7 CFU/mL.

Cell Viability Test. *E. coli* cells were incubated with fresh Gt, GtO, GO or rGO dispersions in isotonic saline solutions at 37 °C under 250 rpm shaking speed for 2 h. The loss of viability of *E. coli* cells was evaluated by colony counting method. Briefly, series of 10-fold cell dilutions (100 μL each) were spread onto LB plates, and left to grow overnight at 37 °C. Colonies were counted and compared with those on control plates to calculate changes in the cell growth inhibition. Isotonic saline solution without graphene-based materials was used as control. All treatments were prepared in duplicate, and repeated at least on three separate occasions.

Cell Morphology Observation. Cell suspensions were dropped on silicon wafers and fixed with 2% glutaraldehyde and 1% osmium tetroxide. Then, *E. coli* cells were dehydrated with sequential treatments by 30, 50, 70, 80, 90, and 100% ethanol for 15 min. The dried cells were sputter-coated with gold for SEM imaging by the JEOL field emission SEM (JSM-6700F).

Detection of Reactive Oxygen Species ($O_2^{\bullet-}$). The possibility of superoxide radical anion ($O_2^{\bullet-}$) production was evaluated by monitoring the absorption of XTT (2,3-bis (2-methoxy-4-nitro-5-sulfophenyl)-2*H*-tetrazolium-5-carboxanilide, Fluka).[31] Details are described in the Supporting Information.

Thiol Oxidation and Quantification. Following the method used in a previous study,[13] the concentration of thiols in GSH was quantified by the Ellman's assay.[37] Gt, GtO, GO, or rGO dispersions (225 μL at 80 μg/mL) in 50 mM bicarbonate buffer (pH 8.6) was added into 225 μL of GSH (0.8 mM in the bicarbonate buffer) to initiate oxidation. All samples were prepared in triplicate. The GSH−Gt, GtO, GO, or rGO mixtures were transferred into a 24-well plate. The 24-well plate was covered with alumina foil to prevent illumination, and then placed in a shaker with a speed of 150 rpm at room temperature for incubation of 2 h. After incubation, 785 μL of 0.05 M Tris-HCl and 15 μL of DNTB (Ellman's reagent, 5,5′-dithio-bis-(2-nitrobenzoic acid), Sigma-Aldrich) were added into the mixtures to yield a yellow product. Gt, GtO, GO, or rGO was removed from the mixtures by filtration through a 0.45 μm polyethersulfone filter (Acrodisc Syringe Filters with Supor Membrane). A 250 μL aliquot of filtered solutions from each sample was then placed in a 96-well plate. Their absorbance at 412 nm was measured on a Benchmark Plus microplate spectrophotometer. GSH solution without graphene-based materials was used as a negative control. GSH (0.4 mM) oxidization by H_2O_2 (1 mM) was used as a positive control. The loss of GSH was calculated by the following formula: loss of GSH % = (absorbance of negative control − absorbance of sample)/absorbance of negative control × 100. After 2 h incubation at the room temperature, 98% of GSH in the positive control sample was lost, which is consistent with previous studies.[13,43]

Acknowledgment. This work was supported by National Research Foundation, Singapore (NRF-CRP2-2007-02 and NRF2010-POC001-021) and Center for Excitonics at Massachusetts Institute of Technology, an Energy Frontier Research Center funded by the U.S. Department of Energy, Office of Science, Office of Basic Energy Sciences under Award Number DE-SC0001088.

Supporting Information Available: Preparation of GO and rGO; characterization of GO samples using Raman spectroscopy and XPS; particle size analysis by dynamic light scattering, control data of cell viability and GSH oxidation experiments; production of superoxide radical anion; comparison of GO and rGO antibacterial activity studies in literatures. This material is available free of charge *via* the Internet at http://pubs.acs.org.

REFERENCES AND NOTES

1. Geim, A. K. Graphene: Status and Prospects. *Science* **2009**, *324*, 1530–1534.
2. Geim, A. K.; Novoselov, K. S. The Rise of Graphene. *Nat. Mater.* **2007**, *6*, 183–191.
3. Novoselov, K. S.; Geim, A. K.; Morozov, S. V.; Jiang, D.; Zhang, Y.; Dubonos, S. V.; Grigorieva, I. V.; Firsov, A. A. Electric Field Effect in Atomically Thin Carbon Films. *Science* **2004**, *306*, 666–669.
4. Park, S.; Ruoff, R. S. Chemical Methods for the Production of Graphenes. *Nat. Nanotechnol.* **2009**, *4*, 217–224.
5. Compton, O. C.; Nguyen, S. T. Graphene Oxide, Highly Reduced Graphene Oxide, and Graphene: Versatile Building Blocks for Carbon-Based Materials. *Small* **2010**, *6*, 711–723.
6. Luo, D. C.; Zhang, G. X.; Liu, J. F.; Sun, X. M. Evaluation Criteria for Reduced Graphene Oxide. *J. Phys. Chem. C* **2011**, *115*, 11327–11335.
7. Rao, C. N. R.; Sood, A. K.; Subrahmanyam, K. S.; Govindaraj, A. Graphene: The New Two-Dimensional Nanomaterial. *Angew. Chem., Int. Ed.* **2009**, *48*, 7752–7777.
8. Yang, K.; Zhang, S.; Zhang, G.; Sun, X.; Lee, S.-T.; Liu, Z. Graphene in Mice: Ultrahigh *in Vivo* Tumor Uptake and Efficient Photothermal Therapy. *Nano Lett.* **2010**, *10*, 3318–3323.
9. Park, S.; Mohanty, N.; Suk, J. W.; Nagaraja, A.; An, J. H.; Piner, R. D.; Cai, W. W.; Dreyer, D. R.; Berry, V.; Ruoff, R. S. Biocompatible, Robust Free-Standing Paper Composed of a TWEEN/Graphene Composite. *Adv. Mater.* **2010**, *22*, 1736–1740.
10. Hu, W. B.; Peng, C.; Luo, W. J.; Lv, M.; Li, X. M.; Li, D.; Huang, Q.; Fan, C. H. Graphene-Based Antibacterial Paper. *ACS Nano* **2010**, *4*, 4317–4323.
11. Akhavan, O.; Ghaderi, E. Toxicity of Graphene and Graphene Oxide Nanowalls against Bacteria. *ACS Nano* **2010**, *4*, 5731–5736.
12. Zhang, Y. B.; Ali, S. F.; Dervishi, E.; Xu, Y.; Li, Z. R.; Casciano, D.; Biris, A. S. Cytotoxicity Effects of Graphene and Single-Wall Carbon Nanotubes in Neural Phaeochromocytoma-Derived PC12 Cells. *ACS Nano* **2010**, *4*, 3181–3186.
13. Vecitis, C. D.; Zodrow, K. R.; Kang, S.; Elimelech, M. Electronic-Structure-Dependent Bacterial Cytotoxicity of Single-Walled Carbon Nanotubes. *ACS Nano* **2010**, *4*, 5471–5479.
14. Kang, S.; Herzberg, M.; Rodrigues, D. F.; Elimelech, M. Antibacterial Effects of Carbon Nanotubes: Size Does Matter. *Langmuir* **2008**, *24*, 6409–6413.
15. Liu, S. B.; Ng, A. K.; Xu, R.; Wei, J.; Tan, C. M.; Yang, Y. H.; Chen, Y. Antibacterial Action of Dispersed Single-Walled Carbon Nanotubes on *Escherichia coli* and *Bacillus subtilis* Investigated by Atomic Force Microscopy. *Nanoscale* **2010**, *2*, 2744–2750.
16. Kang, S.; Pinault, M.; Pfefferle, L. D.; Elimelech, M. Single-Walled Carbon Nanotubes Exhibit Strong Antimicrobial Activity. *Langmuir* **2007**, *23*, 8670–8673.
17. Wang, H. F.; Gu, L. R.; Lin, Y.; Lu, F. S.; Meziani, M. J.; Luo, P. G. J.; Wang, W.; Cao, L.; Sun, Y. P. Unique Aggregation of Anthrax (Bacillus anthracis) Spores by Augar-Coated Single-Walled Carbon Nanotubes. *J. Am. Chem. Soc.* **2006**, *128*, 13364–13365.

18. Arias, L. R.; Yang, L. J. Inactivation of Bacterial Pathogens by Carbon Nanotubes in Suspensions. *Langmuir* **2009**, *25*, 3003–3012.
19. Stankovich, S.; Dikin, D. A.; Piner, R. D.; Kohlhaas, K. A.; Kleinhammes, A.; Jia, Y.; Wu, Y.; Nguyen, S. T.; Ruoff, R. S. Synthesis of Graphene-Based Nanosheets *via* Chemical Reduction of Exfoliated Graphite Oxide. *Carbon* **2007**, *45*, 1558–1565.
20. Petosa, A. R.; Jaisi, D. P.; Quevedo, I. R.; Elimelech, M.; Tufenkji, N. Aggregation and Deposition of Engineered Nanomaterials in Aquatic Environments: Role of Physicochemical Interactions. *Environ. Sci. Technol.* **2010**, *44*, 6532–6549.
21. Saleh, N. B.; Pfefferle, L. D.; Elimelech, M. Aggregation Kinetics of Multiwalled Carbon Nanotubes in Aquatic Systems: Measurements and Environmental Implications. *Environ. Sci. Technol.* **2008**, *42*, 7963–7969.
22. Saleh, N. B.; Pfefferle, L. D.; Elimelech, M. Influence of Biomacromolecules and Humic Acid on the Aggregation Kinetics of Single-Walled Carbon Nanotubes. *Environ. Sci. Technol.* **2010**, *44*, 2412–2418.
23. Chen, K. L.; Elimelech, M. Aggregation and Deposition Kinetics of Fullerene (C60) Nanoparticles. *Langmuir* **2006**, *22*, 10994–11001.
24. Chen, K. L.; Elimelech, M. Interaction of Fullerene (C60) Nanoparticles with Humic Acid and Alginate Coated Silica Surfaces: Measurements, Mechanisms, and Environmental Implications. *Environ. Sci. Technol.* **2008**, *42*, 7607–7614.
25. Lyon, D. Y.; Adams, L. K.; Falkner, J. C.; Alvarez, P. J. J. Antibacterial Activity of Fullerene Water Suspensions: Effects of Preparation Method and Particle Size. *Environ. Sci. Technol.* **2006**, *40*, 4360–4366.
26. Kang, S.; Mauter, M. S.; Elimelech, M. Physicochemical Determinants of Multiwalled Carbon Nanotube Bacterial Cytotoxicity. *Environ. Sci. Technol.* **2008**, *42*, 7528–7534.
27. Liu, S. B.; Wei, L.; Hao, L.; Fang, N.; Chang, M. W.; Xu, R.; Yang, Y. H.; Chen, Y. Sharper and Faster "Nano Darts" Kill More Bacteria: A Study of Antibacterial Activity of Individually Dispersed Pristine Single-Walled Carbon Nanotube. *ACS Nano* **2009**, *3*, 3891–3902.
28. Yang, C. N.; Mamouni, J.; Tang, Y. A.; Yang, L. J. Antimicrobial Activity of Single-Walled Carbon Nanotubes: Length Effect. *Langmuir* **2010**, *26*, 16013–16019.
29. Lyon, D. Y.; Alvarez, P. J. J. Fullerene Water Suspension (*n*C60) Exerts Antibacterial Effects *via* ROS-Independent Protein Oxidation. *Environ. Sci. Technol.* **2008**, *42*, 8127–8132.
30. Lyon, D. Y.; Brunet, L.; Hinkal, G. W.; Wiesner, M. R.; Alvarez, P. J. J. Antibacterial Activity of Fullerene Water Suspensions (*n*C60) Is Not Due to ROS-Mediated Damage. *Nano Lett.* **2008**, *8*, 1539–1543.
31. Ukeda, H.; Maeda, S.; Ishii, T.; Sawamura, M. Spectrophotometric Assay for Superoxide Dismutase Based on Tetrazolium Salt 3′-{1-[(Phenylamino)-carbonyl]-3,4-tetrazolium}-bis(4-methoxy-6-nitro)benzenesulfonic Acid Hydrate Reduction by Xanthine−Xanthine Oxidase. *Anal. Biochem.* **1997**, *251*, 206–209.
32. Joshi, A.; Punyani, S.; Bale, S. S.; Yang, H. C.; Borca-Tasciuc, T.; Kane, R. S. Nanotube-Assisted Protein Deactivation. *Nat. Nanotechnol.* **2008**, *3*, 41–45.
33. Misra, B. R.; Misra, H. P. Vasoactive-Intestinal-Peptide, A Singlet Oxygen Quencher. *J. Biol. Chem.* **1990**, *265*, 15371–15374.
34. Fahey, R. C.; Brown, W. C.; Adams, W. B.; Worsham, M. B. Occurrence of Glutathione in Bacteria. *J. Bacteriol.* **1978**, *133*, 1126–1129.
35. Pompella, A.; Visvikis, A.; Paolicchi, A.; De Tata, V.; Casini, A. F. The Changing Faces of Glutathione, a Cellular Protagonist. *Biochem. Pharmacol.* **2003**, *66*, 1499–1503.
36. Carmel-Harel, O.; Storz, G. Roles of the Glutathione- and Thioredoxin-Dependent Reduction Systems in the *Escherichia coli* and *Saccharomyces cerevisiae* Responses to Oxidative Stress. *Annu. Rev. Microbiol.* **2000**, *54*, 439–461.
37. Ellman, G. L. Tissue Sulfhydryl Groups. *Arch. Biochem. Biophys.* **1959**, *82*, 70–77.
38. McAllister, M. J.; Li, J.-L.; Adamson, D. H.; Schniepp, H. C.; Abdala, A. A.; Liu, J.; Herrera-Alonso, M.; Milius, D. L.; Car, R.; Prud'homme, R. K.; *et al*. Single Sheet Functionalized Graphene by Oxidation and Thermal Expansion of Graphite. *Chem. Mater.* **2007**, *19*, 4396–4404.
39. Dreyer, D. R.; Park, S.; Bielawski, C. W.; Ruoff, R. S. The Chemistry of Graphene Oxide. *Chem. Soc. Rev.* **2010**, *39*, 228–240.
40. Titov, A. V.; Kral, P.; Pearson, R. Sandwiched Graphene-Membrane Superstructures. *ACS Nano* **2010**, *4*, 229–234.
41. Hummers, W. S.; Offeman, R. E. Preparation of Graphitic Oxide. *J. Am. Chem. Soc.* **1958**, *80*, 1339–1339.
42. Kovtyukhova, N. I.; Ollivier, P. J.; Martin, B. R.; Mallouk, T. E.; Chizhik, S. A.; Buzaneva, E. V.; Gorchinskiy, A. D. Layer-by-Layer Assembly of Ultrathin Composite Films From Micron-Sized Graphite Oxide Sheets and Polycations. *Chem. Mater.* **1999**, *11*, 771–778.
43. Winterbourn, C. C.; Metodiewa, D. Reactivity of Biologically Important Thiol Compounds with Superoxide and Hydrogen Peroxide. *Free Radical Biol. Med.* **1999**, *27*, 322–328.